IOPscience iopscience.iop.org

Home Search Collections Journals About Contact us My IOPscience

Electric-field-driven dynamics of magnetic domain walls in magnetic nanowires patterned on ferroelectric domains

This content has been downloaded from IOPscience. Please scroll down to see the full text.

2016 New J. Phys. 18 033027

(http://iopscience.iop.org/1367-2630/18/3/033027)

View the table of contents for this issue, or go to the journal homepage for more

Download details:

IP Address: 91.176.158.140
This content was downloaded on 23/11/2016 at 20:17

Please note that terms and conditions apply.

You may also be interested in:

Logic and memory concepts for all-magnetic computing based on transverse domain walls
J Vandermeulen, B Van de Wiele, L Dupré et al.

A collective coordinate approach to describe magnetic domain wall dynamics applied to nanowires with high perpendicular anisotropy
J Vandermeulen, B Van de Wiele, A Vansteenkiste et al.

Driving large-velocity propagation of ferromagnetic /2 domain walls in nanostripes of cubic-anisotropy materials
Andrzej Janutka, Przemysaw Gawroski and Pawe S Ruszaa

Electric-field control of magnetism via strain transfer across ferromagnetic/ferroelectric interfaces
Tomoyasu Taniyama

Current-induced domain wall motion in nanoscale ferromagnetic elements
G Malinowski, O Boulle and M Kläui

Studies of nanomagnetism using synchrotron-based x-ray photoemission electron microscopy (X-PEEM)
X M Cheng and D J Keavney

New Journal of Physics
The open access journal at the forefront of physics

Deutsche Physikalische Gesellschaft DPG
IOP Institute of Physics

Published in partnership with: Deutsche Physikalische Gesellschaft and the Institute of Physics

OPEN ACCESS

RECEIVED
4 December 2015

REVISED
12 February 2016

ACCEPTED FOR PUBLICATION
1 March 2016

PUBLISHED
16 March 2016

Original content from this work may be used under the terms of the Creative Commons Attribution 3.0 licence.

Any further distribution of this work must maintain attribution to the author(s) and the title of the work, journal citation and DOI.

PAPER

Electric-field-driven dynamics of magnetic domain walls in magnetic nanowires patterned on ferroelectric domains

Ben Van de Wiele[1], **Jonathan Leliaert**[1,2], **Kévin J A Franke**[3] **and Sebastiaan van Dijken**[3]

[1] Department of Electrical Energy, Systems and Automation, Ghent University, Technologiepark 913, B-9052 Ghent-Zwijnaarde, Belgium
[2] Department of Solid State Sciences, Ghent University, Krijgslaan 281/S1, Ghent B-9000, Belgium
[3] NanoSpin, Department of Applied Physics, Aalto University School of Science, PO Box 15100, FI-00076 Aalto, Finland

E-mail: ben.vandewiele@ugent.be **and** sebastiaan.van.dijken@aalto.fi

Keywords: ferroelectric–ferromagnetic heterostructures, magnetic domain wall motion, electric field, magnetic domain wall pinning, nanowires

Supplementary material for this article is available online

Abstract

Strong coupling of magnetic domain walls onto straight ferroelastic boundaries of a ferroelectric layer enables full and reversible electric-field control of magnetic domain wall motion. In this paper, the dynamics of this new driving mechanism is analyzed using micromagnetic simulations. We show that transverse domain walls with a near-180° spin structure are stabilized in magnetic nanowires and that electric fields can move these walls with high velocities. Above a critical velocity, which depends on material parameters, nanowire geometry and the direction of domain wall motion, the magnetic domain walls depin abruptly from the ferroelastic boundaries. Depinning evolves either smoothly or via the emission and annihilation of a vortex or antivortex core (Walker breakdown). In both cases, the magnetic domain wall slows down after depinning in an oscillatory fashion and eventually comes to a halt. The simulations provide design rules for hybrid ferromagnetic–ferroelectric domain-wall-based devices and indicate that material disorder and structural imperfections only influence Walker-breakdown-like depinning at high domain wall velocities.

1. Introduction

Various proposed magnetic memory and logic device concepts rely on the controlled motion of magnetic domain walls through ferromagnetic nanowires [1–3]. Such devices require fast domain wall motion and low power consumption. Magnetic domain walls are conventionally driven by magnetic fields or spin-polarized currents (via the spin-transfer torque effect), but alternatives such as the use of spin Hall currents [4, 5] or electric fields [6] have emerged recently. Electric-field-driven magnetic domain wall motion in the absence of magnetic fields and electric currents can be realized by using magnetoelectric coupling effects [7–9]. One particular attractive scheme relies on elastic pinning of magnetic domain walls on ferroelectric boundaries. This concept, which was experimentally demonstrated for Fe films on $BaTiO_3$ substrates [6], is based on the motion of coupled ferromagnetic–ferroelectric domain wall pairs in an applied electric field. The process is deterministic, fully reversible and, since the current passing through the insulating ferroelectric sub-system is negligible, only requires limited power.

In this work, we investigate the dynamics of magnetic domain walls that are strongly pinned onto ferroelectric boundaries. Dynamic simulations are performed for magnetic nanowires by solving the Landau–Lifshitz–Gilbert equation. The effect of fast ferroelectric domain wall motion is implemented by laterally moving magnetic anisotropy boundaries (ABs). The simulations indicate that near-180° transverse domain walls (TDWs) are stabilized in magnetic nanowires. Strong pinning between magnetic and ferroelectric domain walls persists up to high driving velocities. However, at a critical velocity, depinning occurs. The physics of the depinning process is rich and depends on material parameters, nanowire geometry and the direction of domain wall motion. By varying the anisotropy strength as well as the thickness and width of the ferromagnetic

© 2016 IOP Publishing Ltd and Deutsche Physikalische Gesellschaft

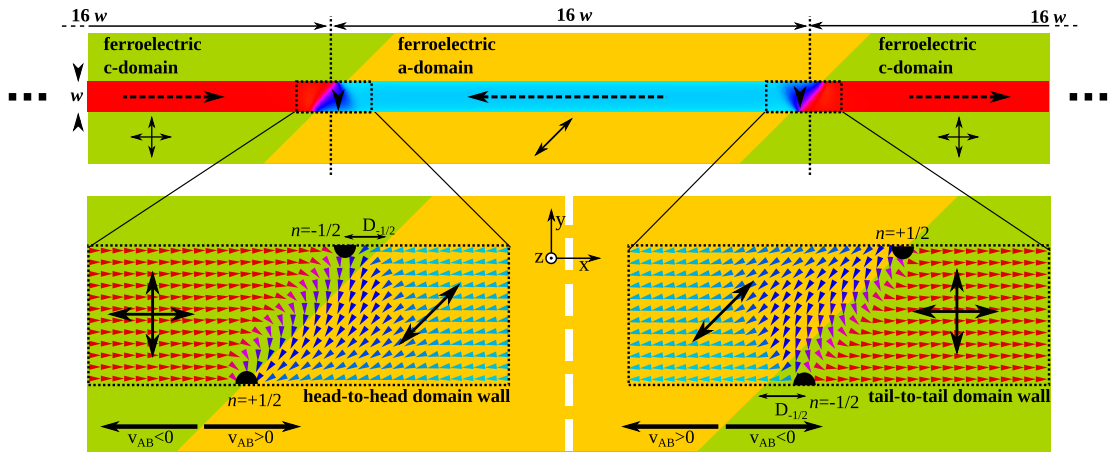

Figure 1. Top: simulated geometry consisting of a nanowire of width w and thickness d. Because of one-dimensional periodic boundary conditions, the simulations are restricted to a length of $32w$. The effect of the ferroelectric substrate is taken into account via strain-induced magnetic anisotropies (indicated by double-headed arrows) that alternate from uniaxial to cubic between stripe domains. Single-headed arrows indicate the magnetization direction in the nanowire. Bottom: simulated micromagnetic configuration. Near-180° TDWs are stabilized on top of the ABs. The domain walls are characterized by a half-vortex ($n = +1/2$) on the ABs and a half-antivortex ($n = -1/2$) at a distance $D_{-1/2}$ from the ABs. The effect of an applied electric field is taken into account by moving the ABs with velocity v_{AB}.

nanowires, we derive optimal conditions for fast domain wall motion and nearly identical domain wall dynamics for positive and negative driving fields. Besides a detailed exploration of magnetic domain wall dynamics in the pinning regime and immediately after depinning, we also explore how material disorder influences electric-field driven magnetic domain wall motion.

2. System and simulation details

We consider a multiferroic heterostructure consisting of a ferroelectric $BaTiO_3$ substrate and a ferromagnetic thin film. The ferroelectric domain structure is characterized by alternating in-plane and out-of-plane polarized stripe domains, *a*- and *c*-domains respectively, separated by narrow ferroelectric domain walls. The ferroelectric polarization in the domains is aligned along the tetragonal lattice elongation, which induces distinct strains in the ferromagnetic film. Due to inverse magnetostriction these strains induce magnetic anisotropies that alternate between uniaxial on top of *a*-domains and cubic on top of *c*-domains [10]. As a consequence, a sharp AB is induced in the ferromagnetic layer at the ferroelectric domain wall. We note the impossibility of inducing similar ABs via a charge accumulation effect in ultrathin ferromagnetic films. The concept of electric-field-driven magnetic domain walls can therefore not be extended to charge-mediated ferromagnetic–ferroelectric bilayers [11, 12].

After patterning the ferromagnetic film into a nanowire with edges along one of the cubic anisotropy axes, i.e. at 45° with the AB, additional magnetic shape anisotropy forces the magnetization to rotate by nearly 180°. The resulting TDWs resemble the ones typically found for in-plane magnetized nanowires with reduced cross sections [13]. The simulated nanowire geometry, illustrating the modulation of magnetic anisotropy and the orientation of magnetization on top of *a*- and *c*-domains, is shown in figure 1.

When applying an out-of-plane electric field across a ferroelectric layer with alternating *a*- and *c*-domains, one type of ferroelectric domain grows at the expense of the other, thereby displacing the ABs and dragging along the TDWs. We simulate the associated magnetization dynamics in a nanowire of width w and thickness d using MuMax3 [14]. The application of an out-of-plane electric field is mimicked by considering laterally moving ABs. Motion at velocity v_{AB} is implemented by shifting the ABs over one discretization cell ($\delta x = 3.125$ nm) during each time window $\delta t = \delta x / v_{AB}$ of the simulations.The computational area is restricted to an *a*-domain and two neighboring *c*-domains (see figure 1). Periodic boundary conditions along the x-direction account for the repetition of this ferroelectric domain pattern. For the ferromagnetic properties, we use experimental data on $Fe/BaTiO_3$ as reference [6]. Input parameters include a saturation magnetization of $M_S = 1.7 \times 10^6$ A m^{-1}, an exchange stiffness of $K_{ex} = 2.1 \times 10^{-11}$ J m^{-1} and a damping constant of $\alpha = 0.01$. First, a 5 nm thick and 200 nm wide nanowire is considered and an uniaxial magnetic anisotropy of $K_u = 2 \times 10^4$ J m^{-3} (on *a*-domains) and a cubic magnetic anisotropy of $K_c = 4 \times 10^4$ J m^{-3} (on *c*-domains) are used. We later vary both the width and thickness of the nanowire and consider magnetic anisotropies of varying strength with $K_c = 2K_u$ and $K_u \in [0.5 \times 10^4$ J m^{-3}, 5×10^4 J m$^{-3}]$. In experimental systems, the induced anisotropy strength depends

on various ferroelectric and ferromagnetic material parameters and the efficiency of strain transfer at the interface. The symmetry of magnetic anisotropy and the anisotropy strengths that we use in the micromagnetic simulations correspond closely to experimental findings for epitaxial Fe films on $BaTiO_3$ crystals with alternating *a*- and *c*-domains [10].

By initializing our simulations as described above, a number of justifiable assumptions are made: (i) ferroelectric domain walls in $BaTiO_3$ can move fast. This assumption is substantiated by experiments [15] and Monte-Carlo simulations [16] indicating domain wall velocities of up to 1000 m s^{-1}. (ii) By using abrupt ABs, we assume that the ferroelectric domain walls in the $BaTiO_3$ substrate are narrow. This is in agreement with experiments and calculations indicating a width of only a few nanometers for 90° ferroelastic domain walls [17, 18]. The width of the strain-induced AB is thus much smaller than the length scale of the TDW that it pins. (iii) Since the domain wall velocities are smaller than the speed of sound in $BaTiO_3$ ($v_{sound} \approx 2000$ m s^{-1} [19]), only quasistatic strain effects are considered. In other words, during ferroelectric domain wall motion the strain state adapts instantaneously to the new polarization direction. The use of moving ABs in the ferromagnetic nanowire with static strain-induced magnetic anisotropies on either side of the ABs does represent this dynamic regime. (iv) Magnetization dynamics does not affect the ferroelectric layer. This assumption is substantiated by considering possible magnetostriction effects. The maximum strain that is generated in the ferromagnetic film via magnetostriction (i.e. by 90° rotation of magnetization) is less than 0.01% for Fe, which is more than two orders of magnitude smaller than the 1.1% lattice tertragonality of $BaTiO_3$. Strain transfer between the ferroelectric and ferromagnetic subsystems is thus highly asymmetric and, as a consequence, magnetostriction does not alter the ferroelectric properties.

3. Results

In the reference nanowire, near-180° TDWs are stabilized on top of the ABs at rest (no electric field applied), as shown in the lower part of figure 1. Identical to conventional nanowire geometries, the TDWs are composed of two edge defects with opposite fractional winding numbers ($n = \pm 1/2$) [20]. At rest, the half-vortex ($n = +1/2$) defect is positioned on top of the ABs and the half-antivortex ($n = -1/2$) defect is slightly shifted into the *c*-domains. This micromagnetic configuration is a compromise between anisotropy energy, which is minimal when the TDWs are pinned onto the ABs, and a reduction of magnetic stray fields.

Figure 2(a) presents the shape of the TDW for different negative v_{AB}'s (domain wall motion in the direction of the *c*-domain). While the TDW follows the displacement of the AB, its relative position is gradually shifted towards the *a*-domain with increasing v_{AB}. This is reflected by a decrease of the distance $D_{-1/2}$ between the half-antivortex and the AB for increasing v_{AB} amplitudes (figure 2(c)). At the same time, the average out-of-plane magnetization component ($\langle m_z \rangle$) in the TDW increases linearly with v_{AB} (figure 2(d)). This behavior is similar to current- and magnetic-field-driven TDW motion in magnetic nanowires. The TDW depins from the AB for $v_{AB} < -315$ m s^{-1}. Once coupling to the AB is lost, the magnetization inside the TDW relaxes back into the film plane via damped oscillations until the wall comes to a stand-still (figure 3(a)). During this process, the velocity v_{TDW} is proportional to the out-of-plane magnetization component in the TDW and v_{TDW} even changes sign when $\langle m_z \rangle$ reverses. This implies that the TDW temporarily moves opposite to the original driving direction. Similar oscillatory relaxations have been experimentally observed for magnetic-field-driven TDWs in half-ring nanowires [21] and can be explained by considering the non-zero mass of magnetic domain walls [21, 22]. A movie of the depinning process is included in the supplementary material.

Also at positive v_{AB}, the TDW follows the AB (figure 2(b)). However, as the AB now moves in the direction of the *a*-domain, the TDW gradually shifts into the *c*-domain with increasing v_{AB}. The distance $D_{-1/2}$ between the half-antivortex and the AB increases up to 80 nm (figure 2(c)). Again, the accompanying out-of-plane magnetization component in the TDW increases with v_{AB} (figure 2(d)). At a critical v_{AB} of 790 m s^{-1}, the half-antivortex emits a $n = -1$ antivortex core into the nanowire and converts into a $+1/2$ defect. In other words, the TDW starts to transform into an antivortex domain wall (see top image in figure 3(d)). For current- or magnetic-field-driven TDWs in nanowires with reduced cross sections, similar transformations take place above Walker breakdown [23–25]. In those cases, the structure of the magnetic domain wall continuously changes between transverse and antivortex states. In contrast, the antivortex domain wall in the electric-field-driven system depins from the AB (see supplemental movie) and thus becomes insensitive to the electrical driving force. As a consequence, the domain wall velocity v_{TDW} drops and the negative $\langle m_z \rangle$ relaxes back into the film plane (figure 3(c)). This relaxation process comprises a recombination of the -1 antivortex core with the recently formed $+1/2$ defect to get back to the original $-1/2$ half-antivortex state. Spin waves are emitted during this annihilation event. While this domain wall relaxation process is much more complex than for negative v_{AB}, the domain wall velocity is again proportional to the out-of-plane magnetization component (figure 3(c)). The

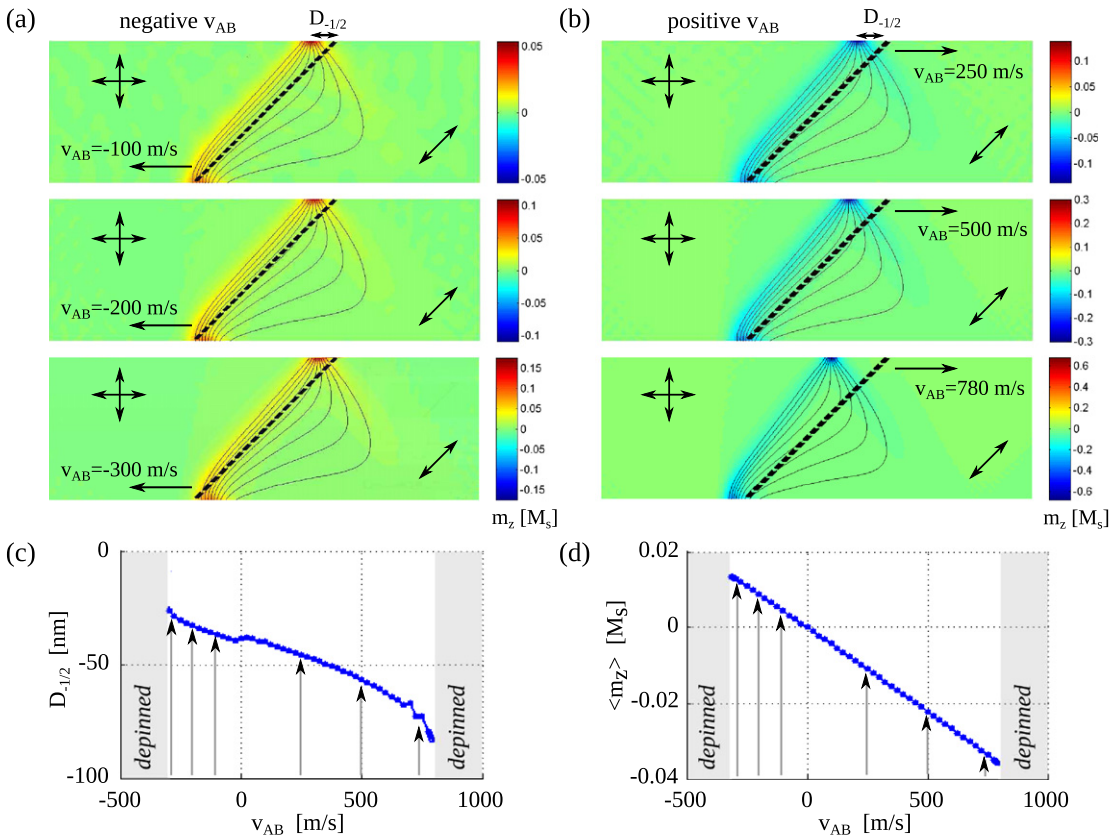

Figure 2. Top panels: magnetization distribution of a moving TDW for (a) negative and (b) positive v_{AB}. Colors represent the out-of-plane magnetization component and the black contour lines indicate variations in m_x. (c) Distance $D_{-1/2}$ between the half-antivortex and the AB and (d) average out-of-plane magnetization component $\langle m_z \rangle$ as a function of v_{AB} for the nanowire with reference parameters.

larger TDW depinning velocity for positive v_{AB} can be attributed to the high energy barrier that needs to be overcome for the creation of an antivortex core.

In figure 4, we summarize the dependence of the depinning velocity (v_{depin}) on ferromagnetic film thickness (d), nanowire width (w) and magnetic anisotropy strength. In all cases, we use a nanowire with a 5 nm $\times$ 200 nm cross section, $K_u = 2 \times 10^4$ J m^{-3} and $K_c = 4 \times 10^4$ J m^{-3} as reference and we change one of the parameters at a time. The relation between the two anisotropies is fixed as $K_c = 2K_u$. For comparison, black data points represent the velocities at which Walker breakdown occurs for magnetic-field-driven TDWs in nanowires with identical geometry and uniform cubic anisotropy, i.e. without ABs (all parameters in these simulations, M_S, K_{ex}, α, and K_c, are identical to those of the c-domain in the ferromagnetic-ferroelectric system). Because of asymmetry in the domain wall shape and the induced magnetic anisotropies, different v_{depin} are obtained for negative and positive v_{AB}. For positive v_{AB}, depinning occurs mostly at velocities that are very similar to the Walker breakdown velocity of magnetic-field-driven TDWs. This close correspondence is explained by the nature of the depinning process, which in both cases encompasses the creation and annihiliation of a vortex or antivortex core, depending on the parameters. In the 5 nm thick reference wire, Walker-breakdown-like behavior sets an upper limit for v_{depin} at about 800 m s^{-1}, irrespective of nanowire width or the magnetic anisotropy strength. Also for negative v_{AB}, the depinning velocity is *Walker-breakdown-limited* if the ferroelectric and ferromagnetic layers are coupled strongly, i.e. for large K_u and K_c (see red data in figure 4(c)).

For parameters where v_{depin} diverges from the black data points in figure 4 the velocity of electric-field-driven TDWs is *coupling-strength-limited*. In these cases, the TDW smoothly depins from the AB before Walker breakdown occurs, as described for negative v_{AB} in our reference wire (see figure 2(a)). Under coupling-strength-limited conditions, v_{depin} increases with increasing nanowire width-to-thickness ratios and magnetic anisotropy strength. This behavior can be understood by considering the effect of these parameters on the out-of-plane magnetization component in the TDW, which, above a certain threshold, triggers domain wall depinning from the AB. Suppression of the out-of-plane tilt by a reduction of stray fields in wide and thin nanowires or an increase of in-plane magnetic anisotropy delays the depinning process.

The simulation results of figure 4 provide clear design rules for hybrid ferromagnetic–ferroelectric domain-wall-based devices. To maximize the velocity at which the TDW and AB remain coupled, one should increase the

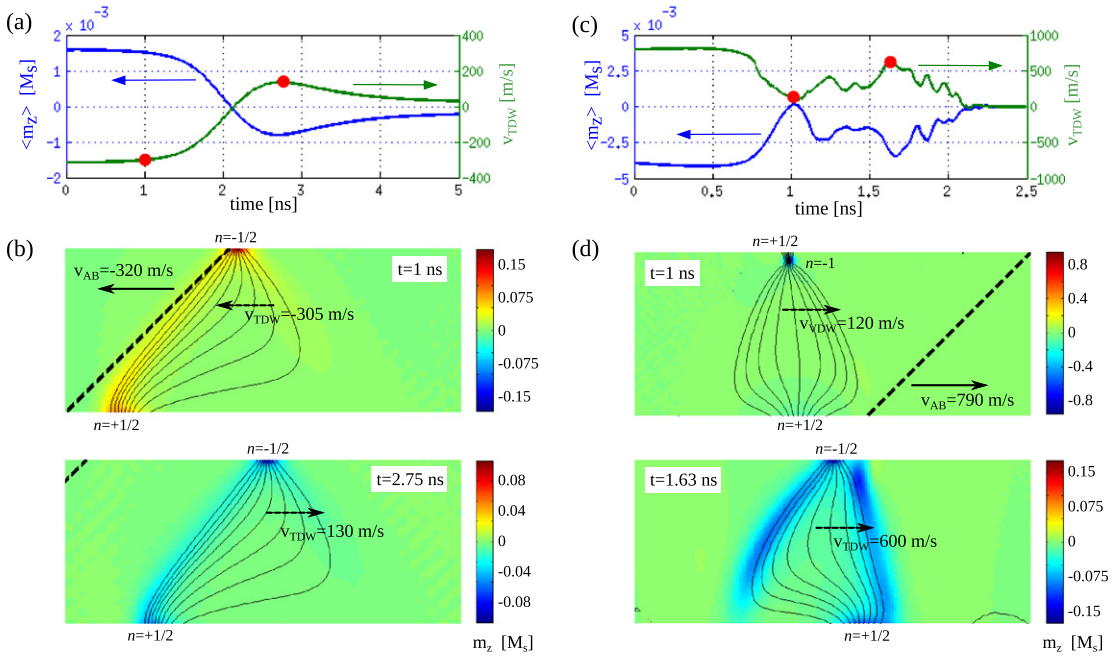

Figure 3. Time evolution of the average out-of-plane magnetization component $\langle m_z \rangle$ in the domain wall (blue, left axis) and the domain wall velocity (green, right axis) after depinning from an AB that moves at (a) $v_{AB} = -320$ m s^{-1} and (c) $v_{AB} = 790$ m s^{-1}. (b) Magnetization distribution in the domain wall at the time points indicated with red circles in (a). At $t = 2.15$ ns, $\langle m_z \rangle$ changes sign and the TDW starts to move in the opposite direction (see bottom panel in (b)). (d) Magnetization distribution in the domain wall at the time points indicated with red circles in (c). A $n = -1$ antivortex core is formed close to the top edge of the nanowire during depinning (see top panel in (d)). Colors represent the local out-of-plane magnetization component and black contour lines indicate variations in m_x.

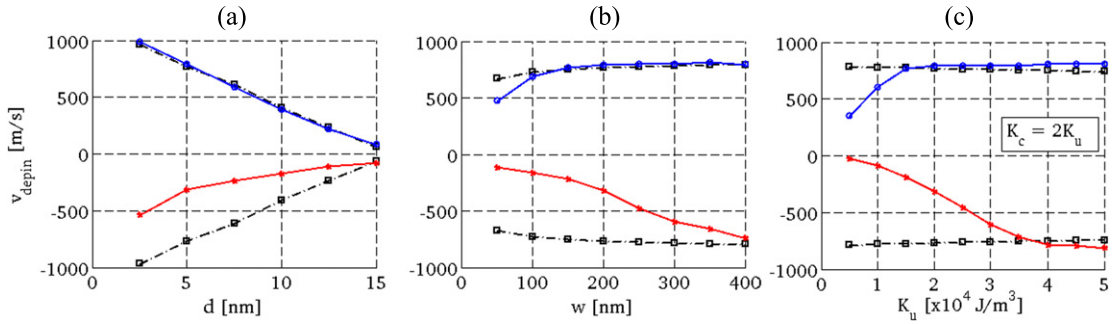

Figure 4. Depinning velocities v_{depin} for TDWs in ferromagnetic nanowires with varying cross-section and induced anisotropy strength (blue and red data points). The reference nanowire has a 5 nm $\times$ 200 nm cross-section and induced anisotropy strengths of $K_u = 2 \times 10^4$ J m^{-3} and $K_c = 4 \times 10^4$ J m^{-3}. Panels (a)–(c) present the influence of nanowire thickness d, width w and induced anisotropy strength (K_u, K_c). One parameter is changed at a time in the simulations. The black data points indicate Walker-breakdown velocities in a nanowire with identical geometry and material parameters, but with *uniform* cubic anisotropy K_c.

magnetic anisotropy or use thin ferromagnetic nanowires. The dependence of TDW dynamics on the direction of motion, which might be undesirable for device applications, is also addressed most efficiently by an increase of magnetic anisotropy strength. For large K_u and K_c, which can be attained by an optimization of interfacial strain coupling, the motion of TDWs becomes Walker-breakdown-limited for both directions. Under strong anisotropy conditions, the thickness and width of the ferromagnetic nanowire can more flexibly be selected without dramatically affecting the maximum TDW velocity.

In our simulations, strong TDW pinning is provided by elastic coupling to an underlying ferroelectric domain wall, enabling electric-field control of the TDW location and velocity. In experiments, material disorder (grain boundaries, impurities) and fabrication imperfections (edge roughness, thickness variations) will introduce additional and randomly distributed pinning potentials. To investigate the influence of such weak disorder on electric-field-driven magnetic domain wall motion, we performed simulations on nanowires with a polycrystalline texture. Structural disorder was implemented by a reduction of the exchange stiffness by 25% at

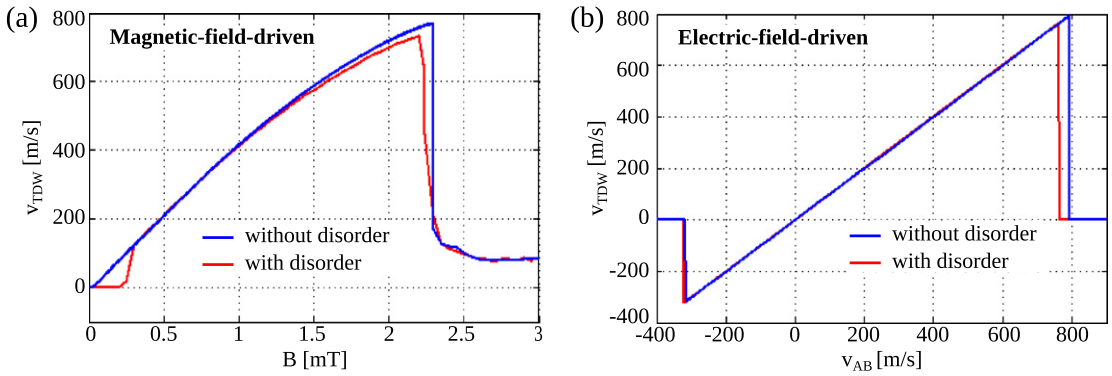

Figure 5. (a) Magnetic-field-driven domain wall motion in a nanowire with uniform cubic anisotropy. Material disorder has two effects: at small fields, the TDW is immobile as it is pinned to disorder and at higher fields disorder expedites Walker breakdown. (b) Electric-field-driven domain wall motion in the reference ferroelectric–ferromagnetic nanowire system. Material disorder has no effect on domain wall motion at small driving fields and it does not influence coupling-strength-limited depinning at negative v_{AB}. Walker-breakdown-like depinning at high positive v_{AB} is affected similarly by disorder as Walker breakdown in magnetic-field-driven nanowires. The nanowire in panel (a) has identical properties as the *c*-domains in the ferroelectric–ferromagnetic nanowire in panel (b).

grain boundaries to account for weaker exchange coupling between grains with a nominal size of 20 nm [26]. This corresponds to local pinning potentials with a depth of about 1 eV, in agreement with experiments [27–29]. Figure 5(a) shows how such disorder influences *magnetic-field-driven* TDW motion (reference nanowire as in figure 4 with uniform cubic anisotropy). At small magnetic driving fields, the TDW does not move at 0 K because of pinning to local disorder. In this dynamic creep regime, magnetic domain walls are activated thermally, leading to stochastic motion via successive pinning/depinning events [30, 31]. Furthermore, structural disorder affects the onset of Walker breakdown as it facilitates the nucleation of (anti)vortex cores [32]. In the *electric-field-driven* ferromagnetic–ferroelectric material system (figure 5(b)), disorder and defects only add small energy perturbations to the strong pinning potentials at the ferroelectric boundaries. Consequently, their influence on magnetic domain wall motion is negligible at small electric driving fields and smooth depinning occurs at the same critical velocity irrespective of the amount of disorder ($v_{depin} = -315$ m s^{-1} in figure 5(b)). Only in the highly dynamical Walker-breakdown-limited pinning regime (large positive v_{AB}), structural disorder effectuates depinning in a way similar to Walker breakdown in magnetic-field-driven nanowires.

The relatively small influence of structural disorder and other imperfections of patterned nanowires on electric-field-driven magnetic domain wall motion is advantageous compared to the use of the spin-transfer torque effect. Another difference relates to power consumption. The spin-transfer torque mechanism requires the application of intense electric currents, leading to considerable power losses via Joule heating. In hybrid ferromagnetic–ferroelectric systems, on the other hand, the current flowing through the insulating ferroelectric layer is negligible. Instead of Joule heating, ferroelectric switching is the primary source of power consumption in this case, which is more energy efficient [6].

4. Conclusions

We numerically investigated fast electric-field-driven magnetic domain wall motion in ferromagnetic nanowires on a ferroelectric $BaTiO_3$ substrate with alternating *a*- and *c*-domains. We show that near-180° TDWs are elastically pinned to the ferroelectric domain boundaries and that they can be moved with velocities up to several 100 m s^{-1}. Depending on the dimension of the nanowire and anisotropy strengths, magnetic domain wall pinning is either Walker-breakdown-limited or coupling-strength-limited. At a critical velocity, magnetic domain walls depin and slow down in an oscillatory fashion. Material disorder and fabrication imperfections only weakly affect the dynamics of electric-field-driven ferromagnetic-ferroelectric domain wall complexes.

Acknowledgments

This work was supported by the Flanders Research Foundation (BVdW), the UGent research fund (BOF project no. 01J16113) (JL), the European Research Council (ERC-2012-StG 307502-E-CONTROL and ERC-PoC-2014 665215-EMOTION) (SvD) and the Academy of Finland (Grant No. 260361) (SvD).

References

[1] Allwood D A, Xiong G, Faulkner C C, Atkinson D, Petit D and Cowburn R P 2005 *Science* **309** 16881692
[2] Parkin S P, Hayashi M and Thomas L 2008 *Science* **320** 190–4
[3] Omari K A and Hayward T J 2014 *Phys. Rev. Appl.* **2** 044001
[4] Ryu K S, Thomas L, Yang S H and Parkin S 2013 *Nat. Nanotech.* **8** 527–33
[5] Emori S, Bauer U, Ahn S M, Eduardo M and Beach G S D 2013 *Nat. Mater.* **12** 611–6
[6] Franke K J A, Van de Wiele B, Shirahata Y, Hämäläinen S J, Taniyama T and van Dijken S 2015 *Phys. Rev.* X **5** 011010
[7] Chung T K, Carman G P and Mohanchandra K P 2008 *Appl. Phys. Lett.* **92** 112509
[8] Lahtinen T H E, Franke K J A and van Dijken S 2012 *Sci. Rep.* **2** 258
[9] Parkes D E, Cavill S A, Hindmarch A T, Wadley P, McGee F, Staddon C R, Edmonds K W, Campion R P, Gallagher B L and Rushforth A W 2012 *Appl. Phys. Lett.* **101** 072402
[10] Lahtinen T H E, Shirahata Y, Yao L, Franke K J A, Venkataiah G, Taniyama T and van Dijken S 2012 *Appl. Phys. Lett.* **101** 262405
[11] Hu J M, Nan C W and Chen L Q 2011 *Phys. Rev.* B **83** 134408
[12] Vaz C A F 2012 *J. Phys.: Condens. Matter* **24** 333201
[13] Nakatani Y, Thiaville A and Miltat J 2005 *J. Magn. Magn. Mater.* **290-291** 750–3
[14] Vansteenkiste A, Leliaert J, Dvornik M, Helsen M, Garcia-Sanchez F and Van Waeyenberge B 2014 *AIP Adv.* **4** 107133
[15] Stadler H L and Zachmanidis P J 1963 *J. Appl. Phys.* **34** 3255–60
[16] Shin Y H, Grinberg I, Chen I W and Rappe A M 2007 *Nature* **449** 881–4
[17] Hlinka J and Márton P 2006 *Phys. Rev.* B **74** 104104
[18] Zhang Q and Goddard W A 2006 *Appl. Phys. Lett.* **89** 182903
[19] Tagantsev A K, Fousek J and Cross L E 2010 *Domains in Ferroic Crystals and Thin Films* (Berlin: Springer)
[20] Tchernyshyov O and Chern G W 2005 *Phys. Rev. Lett.* **95** 197204
[21] Rhensius J, Heyne L, Backes D, Krzyk S, Heyderman L J, Joly L, Nolting F and Kläui M 2010 *Phys. Rev. Lett.* **104** 067201
[22] Thomas L, Moriya R, Rettner C and Parkin S S 2010 *Science* **330** 1810–3
[23] Schryer N L and Walker L R 1974 *J. Appl. Phys.* **45** 5406–21
[24] Thiaville A and Nakatani Y 2006 *Spin Dynamics in Confined Magnetic Structures III* (*Topics in Applied Physics* vol 101) (Springer: Berlin) pp 61–205
[25] Lee J Y, Lee K S, Choi S, Guslienko K Y and Kim S K 2007 *Phys. Rev.* B **76** 184408
[26] Leliaert J, Van de Wiele B, Vansteenkiste A, Laurson L, Durin G, Dupré L and Van Waeyenberge B 2014 *J. Appl. Phys.* **115** 17D102
[27] Kim J S *et al* 2010 *Phys. Rev.* B **82** 104427
[28] Chen T Y, Erickson M J, Crowell P A and Leighton C 2012 *Phys. Rev. Lett.* **109** 097202
[29] Burgess J A J, Fraser A E, Sani F F, Vick D, Hauer B D, Davis J P and Freeman M R 2013 *Science* **339** 1051–4
[30] Cayssol F, Ravelosona D, Chappert C, Ferre J and Jamet J P 2004 *Phys. Rev. Lett.* **92** 107202
[31] Metaxas P 2010 *Creep and Flow Dynamics of Magnetic Domain Walls: Weak Disorder, Wall Binding, and Periodic Pinning* (*Solid State Physic* vol 62) (New York: Academic) pp 75–162
[32] Leliaert J, Van de Wiele B, Vansteenkiste A, Laurson L, Durin G, Dupré L and Van Waeyenberge B 2014 *J. Appl. Phys.* **115** 233903